T. J. Wang
State Key Laboratory of Nonlinear Mechanics,
Institute of Mechanics,
Chinese Academy of Sciences,
Beijing 100190, China;
School of Engineering Science,
University of Chinese Academy of Sciences,
Beijing 100049, China
e-mail: wtjing@126.com

J. F. Nie
Institute of Nuclear and New Energy Technology,
Tsinghua University,
Beijing 100084, China
e-mail: niejf@tsinghua.edu.cn

Q. Peng[1]
State Key Laboratory of Nonlinear Mechanics,
Institute of Mechanics,
Chinese Academy of Sciences,
Beijing 100190, China;
School of Engineering Science,
University of Chinese Academy of Sciences,
Beijing 100049, China
e-mail: qpeng@imech.ac.cn

X. Liu[1]
State Key Laboratory of Nonlinear Mechanics,
Institute of Mechanics,
Chinese Academy of Sciences,
Beijing 100190, China;
School of Engineering Science,
University of Chinese Academy of Sciences,
Beijing 100049, China
e-mails: xiaomingliu@imech.ac.cn;
Xiaomingliu@lnm.imech.ac.cn

Y. G. Wei
College of Engineering,
Peking University,
Beijing 100871, China
e-mail: weiyg@pku.edu.cn

Frictional Detachment Between Slender Whisker and Round Obstacle

In nature, hair-like whiskers are used to detect surrounding information, such as surface texture and air flow field. The detection requires a comprehensive understanding of the relationship between whisker deformation and the contact force. With a whisker being modeled as a slender beam, the contact problem cannot be solved by small deformation beam theory and thus requires a new mechanical model to build up the relationship between whisker deformation and the contact force. In this work, the contact problem between a whisker and a round obstacle is solved, considering three factors: large deformation of the whisker, size of the obstacle, and frictional effect of the interface. Force and energy histories during the contact are analyzed under two motion modes: translation and rotation. Results show that the rotational mode is preferred in nature, because rotation of a whisker over an obstacle requires less energy for frictional dissipation. In addition, there are two types of detachment during the slip between the whisker and the obstacle. The detachment types are dependent on the whisker's length and can be explained by the buckling theory of a slender beam. [DOI: 10.1115/1.4047627]

Keywords: whisker modeling, obstacle contact, frictional detachment, large deformation beam theory, computational mechanics, elasticity

1 Introduction

Hair-like structures (whiskers), such as the antennas of insects or the vibrissae of mammals, provide an efficient way for living beings to communicate with their surroundings. The mechanical interaction between the whiskers and surrounding obstacles will be converted into chemical signals, so that the neurons can use the signals for deciding the tactile action. For example, Krupa et al. [1] studied the facial whiskers of rats, and results indicated that the trigeminal somatosensory system forms internal representations of external stimuli by integrating tactile input from multiple facial whiskers. During whisking, the spatial coordinates are encoded by neuronal variables [2], and environmental information such as air flow can be acquired by hair-like sensilla. Such mechanical stimuli have been studied with the help of mathematical models [3]. Understanding the mechanical interaction of living beings with the environment will shed a light on soft-robot design [4,5]. Robotic whiskers [6] are used for tactile sensing technology and show potential application in navigation, obstacle avoidance, and surface texture detection.

It is necessary to build up a whisker contact model to determine the mechanism of information acquisition by sensory organs under mechanical stimuli. The whisker is a flexible beam with one free end contacting with obstacle and can be used to extract surface information by detecting the contact position [7]. In this work [7], they assumed that the whisker only made side contact with the object during slip, and the results can be used for developing functional tactile robots [6]. Other researchers [6–9] used various mechanical factors such as rotational stiffness, bending or torque moment, and bending or torque angle to characterize the contact status. Subsequently, Solomon and Hartmann [6,10] proposed a localization method to solve the contact problem numerically. In their model [6], the beam was simulated using n nodes by linear interpolation. The shape of the whisker was obtained by solving

the governing equation of classical beam. In a similar way, but only for small deformation, Birdwell et al. [9] used the small deflection theory to establish an analytical model. This method only considered small deflections of the beam and thus cannot provide a general solution for a large deformed whisker. Considering the larger angular deflection, other studies used built-in subroutine of MATLAB (MathWorks, USA) to solve the boundary value problem [9,11]. In addition, the finite element method [12] was also conducted to build up the connection between the mechanical characteristics of flexible probes and surface topology. However, the finite element model is built on a case-by-case basis and is thus unable to form a general solution. In another study [13], a similar contact problem was solved by using the boundary value problem of the Euler–Bernoulli beam theory, in which the authors built up a set of differential equations with boundary conditions at the whisker base and the contact condition at the whisker top. The differential equations were solved numerically in MATLAB using *ode45*. Likewise, Hires et al. [14] used the boundary value problem solver software package XPPAUT and the embedded AUTO package to compute bifurcation solutions of a whisker contact. The iterative shooting method was used to solve the equation numerically. The application of this method provided a theoretical understanding for the sliding phenomenon of the contact. As in Hires et al.'s model [14], by using the iterative shooting method, a detailed analysis of the contact between a slender beam and an obstacle was provided.

However, there are three issues requiring attention: the frictional contact of the interface [15], the size effect of the object [14], and the relative motion type between the beam and the obstacle. All previous studies are limited to rotation, without considering translation.

Another interesting point is the detachment type between the whisker and the obstacle. The different detachments are derived from the fact that there are usually multiple solutions for the boundary value problem of whisker contact. In the study by Hires et al. [14], the saddle point bifurcation of the boundary value problem was explained. In addition, Maoiléidigh et al. [16] established a mechanical model of the hair-like structure considering factors such as stiffness, damping, mass, and force loads. In this study, the beam was considered to have three different adaptive states, i.e., monostable, bistable, and self-oscillating, depending on the mechanical loading of the system.

In the present study, a whisker contact model considering large deformation was developed to study the frictional detachment between a whisker and a round obstacle. Finite element simulation was conducted to verify the proposed model. The effect of interfacial friction and obstacle size on the frictional detachment style was studied using the developed model. The evolution of contact force and energy dissipation during the detachment was analyzed to provide the evidence of energy-preferred detachment style (translation or rotation). Results were compared to illuminate the difference between the translational mode and the beam-pedestal interaction model in the three-point bending test [17].

2 Modeling Method

2.1 Model of Whisker Contact With an Obstacle. Figure 1 illustrates the physical process for the contact problem between a whisker and an obstacle. The whisker was modeled with a slender beam and a rigid disk as an obstacle. The translation mode was realized by fixing the displacement in the *x* direction and displacing the left end of the whisker in the *y* direction. The rotation mode was realized by fixing the displacement in the *x* and *y* directions and rotating the whisker counterclockwise against the rigid obstacle.

The details of the whisker contact model, including geometry, material model, and boundary conditions, are presented in this section. As shown in Fig. 2, the obstacle was assumed to be a cylindrical pole perpendicular to the motion plane. This assumption was similar to that in the whisker-obstacle contact experiments. Thus, in the present model, sliding of the whisker along the *z*-axis was not
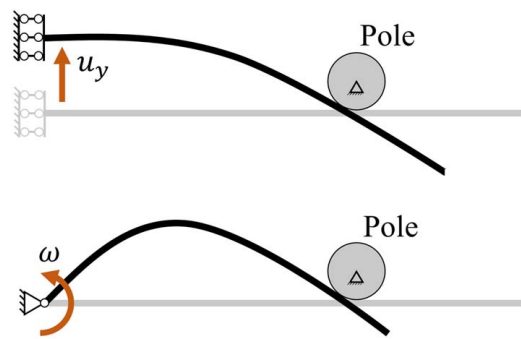

Fig. 1 Sketch of contact model

considered, so the contact between the whisker and the object was limited to the *x-y* plane. The obstacle was assumed to be rigid, while the whisker was assumed to be a linear elastic beam, with equal cross sections. For the interaction between whisker and obstacle, we considered two typical modes, i.e., translation and rotation, which are shown in Figs. 2(a) and 2(b), respectively.

Large deformation is important for a whisker to achieve tactile function, so in this study, a mechanical model was used for a largely deformed whisker, which is crucial for simulating the contact process. In the previous study on biological hire-like structures [5], the slenderness ratio (length over radius) ranged from 10 to 1000. For such a high slenderness ratio value, the whisker deformed with very large rotation angle during the contact. As a result, the small deflection theory was not suitable, and the large deformation theory of the beam should be used instead [18].

In the following, the reasons that the obstacle size and interfacial friction should be considered in the present model are discussed. The previous studies [9,15] considered contact between whisker and obstacle as a point load, and this assumption deviated slightly for small obstacles. However, for large obstacles, this deviation was significant as indicated by Hires et al. [14]. In their model [14], the size of the obstacle was considered, yet a frictionless contact model was used. However, a similar test showed that friction has a strong effect during contact between a large deflection beam and the pedestal in three-point bending [17]. This conclusion implies that friction should also be considered in the contact model dealing with a slender whisker and an obstacle. Here, to model the stable slip, the Coulomb friction law with a constant coefficient was used.

As shown in Fig. 2, the geometry and boundary conditions were provided as follows. The whisker was considered to be a straight beam with a uniform section, similar to human hair or seal whiskers, and the initial curvature was ignored. The coordinate system was defined as shown in Fig. 2: the moving end was set at the origin, while the positive *y* direction was defined as opposite to the translation direction; the rotation angle of the constrained end was defined as θ_0, and the positive direction of which was counterclockwise. The coordinates along the *x* and *y* axes of the beam were functions of arc length *s* and angle θ between the tangential direction of the beam and positive direction of the *x*-axis was also a function of arc length *s*. The total length of the beam was L_w, while the initial distance between contact point and origin was *L*. The obstacle had a radius R_{pole}, and obstacle's center was defined at the point (x_{cen}, y_{cen}). The size coefficient *m* was introduced by $m = R_{pole}/L$, indicating the size of the obastcle nondimensionalized by the distance from detection point.

In Secs. 2.2 and 2.3, the length of the slender beam L_w/L is kept as a constant 3.0. To check the effect of obstacle size and interfacial friction, we study the obstacles with size coefficient $m = 0.1, 0.5$ and the interface with friction coefficient $\mu = 0.0, 0.2$. In Sec. 3.3, we change the length of the whisker to study the length-dependent detachment.

During contact, the contact force is applied at the point of the beam with an arc length S_{obj}. Figure 2(c) shows the geometric
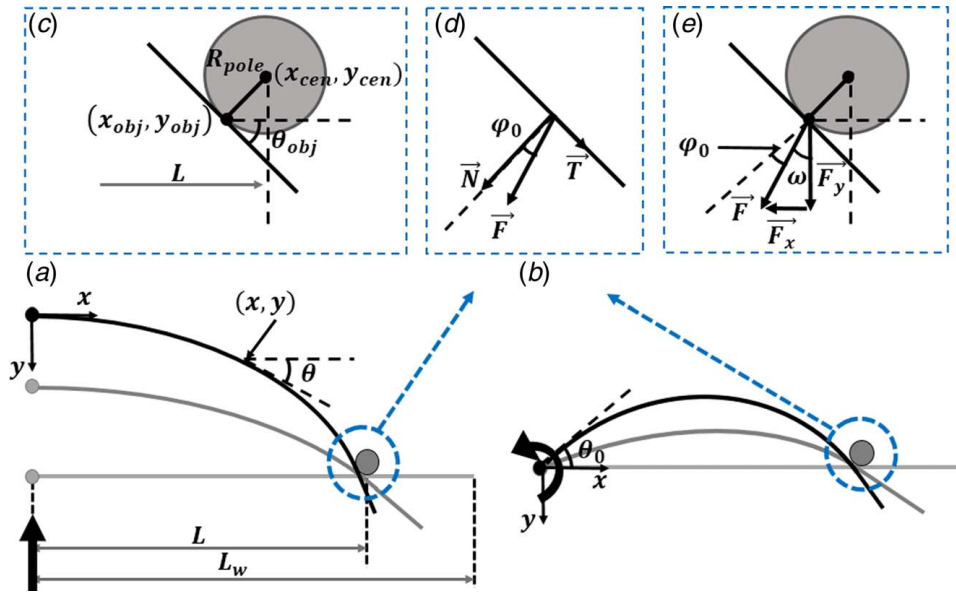
Fig. 2 Sketch of contact between whisker and obstacle in two dimensions: (a) translation model, (b) rotation mode, (c) magnification at contact point, (d) resultant forces decomposed in normal and tangential directions of contact surface, and (e) resultant forces decomposed in global coordinates

coordinate relationship between the contact point and object center, which can be expressed by

$$x_{obj} = x_{cen} - mL \sin \theta_{obj} \qquad (1)$$

$$y_{obj} = y_{cen} + mL \cos \theta_{obj} \qquad (2)$$

where θ_{obj} is defined as the object angle as shown in Fig. 2(c). The contact force F can be decomposed into F_x and F_y or T and N in the coordinates as shown in Figs. 2(d) and 2(e):

$$|F| = \sqrt{F_x^2 + F_y^2} = \sqrt{N^2 + T^2} \qquad (3a)$$

$$\frac{F_x}{F_y} = \tan \omega \qquad (3b)$$

$$\frac{T}{N} = \tan \varphi_0 \qquad (3c)$$

where μ is the friction coefficient and φ_0 is the friction angle. In addition, the geometric relationship shown by Fig. 2(e) directly leads to the relation between ω and φ_0:

$$\omega = \theta_{obj} - \varphi_0 \qquad (4)$$

In the deformation analysis of a whisker [19], the relationship between moment and curvature can be expressed as follows:

$$\frac{d\theta}{ds} = \frac{M(s)}{EI(s)} \qquad (5)$$

where θ is the bending angle and $M(s)$ can be calculated by

$$M(s) = F_y(x_{obj} - x_s) - F_x(y_{obj} - y_s) \qquad (6)$$

The bending stiffness of the beam is $EI(s)$, where E is the modulus and $I(s)$ the moment of inertia of the beam section about the neutral axis. The geometric relations can be expressed by

$$\frac{dx}{ds} = \cos \theta \qquad (7a)$$

$$\frac{dy}{ds} = \sin \theta \qquad (7b)$$

By solving Eqs. (4)–(7), we can obtain the integral expression for arc length s in terms of θ, θ_{obj}, φ_0, and F:

$$\frac{s}{L} = \frac{1}{2\sqrt{\alpha}} \int_{\theta_0}^{\theta} \frac{dt}{\sqrt{g(\theta_{obj}, \varphi_0) + f(\theta_{obj}, \varphi_o, t)}} \qquad (8a)$$

The coordinates (x, y), as a function of s, can be then expressed by

$$\frac{x}{L} = \frac{1}{2\sqrt{\alpha}} \int_{\theta_0}^{\theta} \frac{\cos t \, dt}{\sqrt{g(\theta_{obj}, \varphi_0) + f(\theta_{obj}, \varphi_o, t)}} \qquad (8b)$$

$$\frac{y}{L} = \frac{1}{2\sqrt{\alpha}} \int_{\theta_0}^{\theta} \frac{\sin t \, dt}{\sqrt{g(\theta_{obj}, \varphi_0) + f(\theta_{obj}, \varphi_o, t)}} \qquad (8c)$$

where

$$\alpha = \frac{FL^2}{2EI} \qquad (8d)$$

$$g(\theta_{obj}, \varphi_0) = \left[\cos(\theta_{obj} - \varphi_0) \sin \theta_{obj} - \sin(\theta_{obj} - \varphi_0) \cos \theta_{obj} \right] \qquad (8e)$$

$$f(\theta_{obj}, \varphi_0, t) = \sin \theta_{obj} \cos t - \cos \theta_{obj} \sin t \qquad (8f)$$

The governing Eqs. 8(a)–8(f) can be solved by using proper boundary conditions and geometric relations Eqs. (1) and (2). The boundary conditions are dependent on the motion mode, as follows.

For the translation mode, the boundary conditions are as follows:

$$s = 0: \quad x(0) = 0, \quad y(0) = 0, \quad \theta(0) = 0$$

$$s = s_{obj}: \quad x(s_{obj}) = (1 - m\sin\theta_{obj})L, \quad y(s_{obj}) = y_{cen} + y_{tran}$$
$$+ mL\cos\theta_{obj}, \quad \theta(s_{obj}) = \theta_{obj}$$

For the rotation mode, the boundary conditions are as follows:

$$s = 0: \quad \theta(0) = \theta_0$$

$$s = s_{obj}: \quad y(s_{obj}) = y_{cen} + mL\cos\theta_{obj}$$

where y_{tran} and θ_0 are the two control parameters, which are the relative displacement under the translation mode and the relative rotation angle under the rotation mode, respectively. With increasing y_{tran} or θ_0, the complete solution of contact forces can be obtained by solving Eqs. 8(a)–8(f) using the iterative shooting method with proper boundary conditions. The iterative shooting method is an algorithm used to solve the boundary value problem and determine the initial value by the method of gradual approximation and is realized by the built-in function *fsolve* of MATLAB. The MATLAB script used for solving the present boundary value problem can be downloaded online.[2]

In this study, the evolution of force and energy during the contact process is studied to determine which mode is more efficient. The external work for the two motion modes is calculated, respectively, as follows:

$$W = \int_0^{y_{tran}} F_y \, dy \tag{9a}$$

$$W = \int_0^{\theta_0} M \, d\theta \tag{9b}$$

Equation (9a) represents the external work for the translation mode, while Eq. (9b) represents that for the rotation mode. The total strain energy of the beam can be expressed as follows:

$$U = \int_0^s \frac{M^2}{2EI} \, ds \tag{10}$$

In addition, the frictional energy is expressed as follows:

$$U_f = W - U \tag{11}$$

There are two different ways that frictional detachment between a whisker and an obstacle occurs. In Hires et al.'s [14] study on the rotation motion between a conical whisker and obstacle, two different detachment styles were defined: "pull-off" due to the contact arc length reaching the beam length and "slip-off" due to the instability slip of the beam. To show the effects of obstacle size and interfacial friction on the detachment, we studied slip processes between whisker and obstacle by solving Eqs. 8(a)–8(f) numerically for both translation and rotation modes.

2.2 Verification With Finite Element Model. To verify the present model, we build up a similar finite element model, with a beam contacting a round obstacle. Contact nonlinearity [9,11,12] can be solved numerically by using the finite element method. In the finite element model, because the normal force from Hertz contact has a nonlinear relation with penetration distance to the power of 1.5, it is assumed that the contact stiffness is much larger than the stiffness of the beam. Based on this assumption, the obstacle is considered to be rigid. The material of beam is assumed to be linearly elastic, with a modulus of 200 GPa and a Poisson ratio of 0.3.

As with the same boundary in Sec. 2.1, in the finite element model, the movement of the whisker is constrained in two dimension, sliding along the *z*-axis is not considered, as shown in Fig. 2. The whisker has a length of 300 mm, and the arc length at
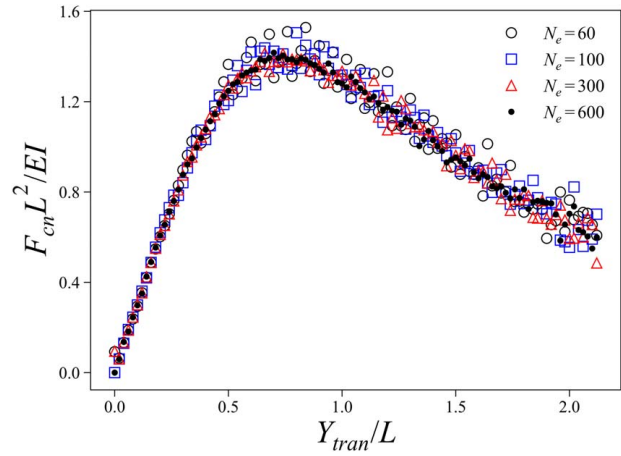
Fig. 3 Mesh dependency check for the finite element model

the initial contact point is 100 mm, so in the finite element simulation, the value of L_w/L is set as 3.0, as shown in Fig. 2. The section of the beam is circular, the radius of which is 1/20 of the total length. Element type for the whisker is set to B21, a built-in beam element in the commercial ABAQUS software. Meshes with elemental count up to 600 were also checked. Figure 3 shows the relationship between normal contact force and translation displacement for models with various elemental counts (60, 100, 300, and 600). Result shows consistency in the mesh study. In this study, a mesh with 300 beam elements was adopted for computational efficiency.

The contact in the normal direction is defined as hard contact using penalty functions, and the contact in the tangential direction is set as Coulomb friction. Two friction coefficients were chosen ($\mu = 0$, $\mu = 0.2$) to study the frictional effect. For studying the size effect, two sizes of obstacle ($R_{pole} = 10$ mm and 50 mm) were chosen, so that the size coefficients ($m = R_{pole}/L$) are 0.1 and 0.5, respectively. Finally, the explicit solver of ABAQUS was used to carry out the simulation. The boundary conditions for both rotation mode and translation modes are the same as detailed in Sec. 2.1.

Since all the parameters in the derivation in Sec. 2.1 are normalized, the final results are independent on the choice for both material properties and geometry. The comparison between the model presented in Sec. 2.1 and finite element method in this section is shown in Fig. 4. In Figs. 4(a) and 4(b), the comparison of reaction forces in two directions under the translation mode shows good agreement, for different obstacle sizes and friction coefficients. In Fig. 4(c), the comparison of the reaction moment under the rotation mode also gives good agreement.

3 Results and Discussion

3.1 Two Types of Detachment. To study the detachment, we simulated the slip of the whisker with length $L_w = 3L$ in two different modes. In Fig. 5, three snapshots during the detachment are shown: one at the beginning, one at the middle of slip, and one at the time of slip. In the translation mode as shown in Figs. 5(a)–5(c), the detachment is typical "pull-off," which is due to the contact arc length exceeding the beam length. For the rotation mode as shown in Figs. 5(b)–5(d), the detachment is typical "slip-off," which is due to the instable slip of the whisker. The effects of obstacle size and interfacial friction are checked by choosing, $\mu = 0$, $\mu = 0.2$ and $m = 0.1$, $m = 0.5$, respectively. It is found that detachment style does not change with obstacle size and friction state. The style is mainly dependent on the whisker length, which is discussed in Sec. 3.3.

3.2 Evolution of Strain Energy and Friction Dissipation During Contact. In this section, to check the effect of obstacle size and friction state, we study an initial beam with
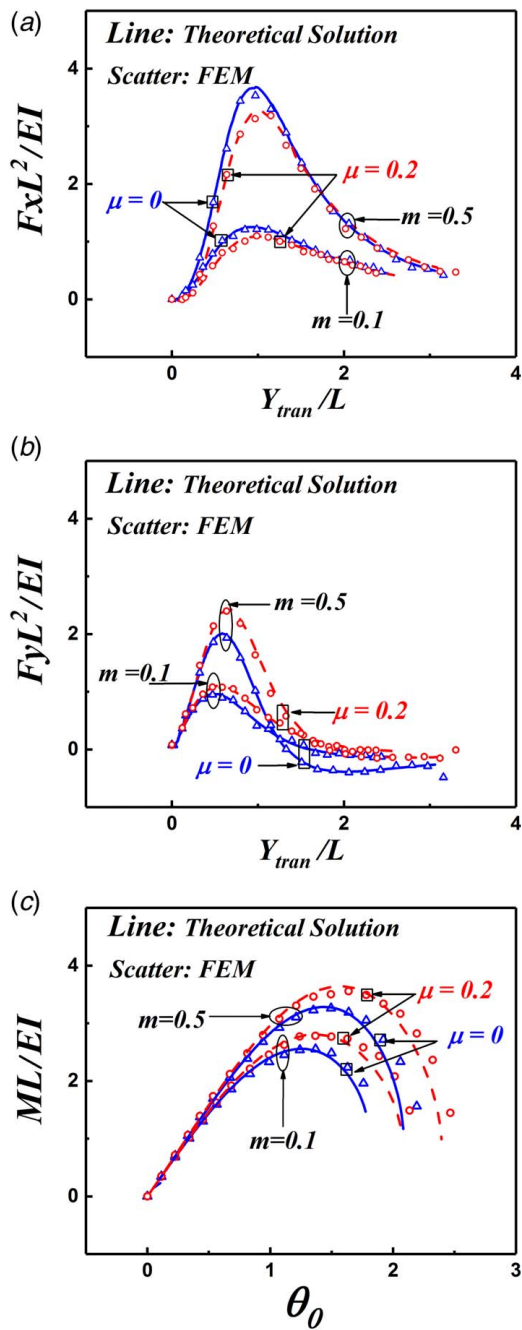
Fig. 4 Comparison of solutions obtained in this study with finite element results in translation and rotation modes: (a) contact force in x direction with respect to translation displacement, (b) contact force in y direction with respect to translation displacement, and (c) bending moment with respect to rotation angle at fixed end

length $L_w = 3L$, contacting the obstacle with $m = 0, 0.1, 0.5$. During sliding, the friction coefficient was chosen as follows: $\mu = 0, 0.2$. The passing process of one whisker over an obstacle is conducted by using the MATLAB script.[3] The simulation stops when the whisker has passed the obstacle.

The energy required to pass over the object is important for the whisker contact. The evolutions of external work and strain energy for two modes are shown in Figs. 6 and 7, in which the work or energy is divided by EI/L and the displacement is

divided by L. From Figs. 6 and 7, the effects of obstacle size and friction coefficient are different for the two modes, as follows.

(1) For the translation mode, the external work required for passing an obstacle is sensitive to the obstacle size and friction coefficient. A larger obstacle requires much more external work for the whisker to pass over it. For instance, as shown in Fig. 6, the larger obstacle ($m = 0.5$) with friction requires twice the external work than the smaller obstacle ($m = 0.1$) without friction. The stored strain energy shows similar trends, as shown in Fig. 7.
(2) For the rotation mode, external work, as well as strain energy, shows little dependence on the obstacle size and the friction coefficient during contact. The external work shows less than a 20% difference between the smaller obstacle ($m = 0.1$) without friction and the larger obstacle ($m = 0.5$) with friction.

To determine the friction dissipation during contact, we plot the ratio of friction dissipation to the external work as shown in Figs. 8(a) and 8(b). A large amount of energy is dissipated by friction in the translation mode, more than 30% is dissipated in the case of a small obstacle ($m = 0.1$) and more than 50% is dissipated in the case of a large obstacle ($m = 0.5$). However, the situation is different for the rotation mode during contact: less than 10% of energy is dissipated by friction for both small and large obstacles, and friction dissipation is not sensitive to the obstacle size in the rotation mode. Thus, it is concluded that the rotation mode is more preferred in nature because it is more energy efficient.

Imaging in the macro-scale, one must know the macro-scale friction of a bundle of whiskers sliding over a rough surface with identical obstacles. The single whisker-obstacle contact model can be used to obtain the macro-scale friction coefficient between one rough surface and one randomly distributed bundles: the rough surface consists of identical obstacles (same R_{pole}), and the bundles consist of randomly distributed whiskers with the same height (same L_w/L). This interpretation of macro-scale friction coefficient is consistent with the averaging method in statistical mechanics; that is, it expresses macroscopic quantities of the system as a statistical average of microscopic function. In statistical mechanics, such an average can be replaced by an average over one simulation period if, in the simulation, the fraction of time the system spends in each state satisfying a Boltzmann's distribution. For the friction problem, we assume that the rough surfaces are sufficiently large such that all pair configurations have the same probability to be found. Therefore, we can replace the ensemble average with the distance average of one simulation.

Taking a statistical average, the macro friction coefficient can be obtained by the following expression:

$$\mu_{macro} = \frac{\int F_y dy}{\int F_x dy} \tag{12}$$

By using Eq. (12), the macro friction coefficient can be plotted as shown in Fig. 9. With the present parameters, a large μ_{macro} (more than 0.2) can be obtained with a microscale frictionless bundle ($\mu = 0.0$). What is more important is that μ_{macro} shows a clear dependence on the obstacle size, with the trend that bigger is smoother.

3.3 Length-Dependent Detachment. In this section, simulations were conducted to check the length effect of the whisker on the detachment. The length is critical for determining two frictional detachments between a whisker and an obstacle: "pull-off" due to the contact arc length reaching the beam length and "slip-off" due to the instability slip of the beam.

3.3.1 Transition From "Pull-Off" to "Slip-Off". To study the transition from "pull-off" detachment to "slip-off" detachment, we conducted a simulation with the increasing whisker length, starting from $L_w = L$. The $d_{critical}$ is defined as the value of displacement at
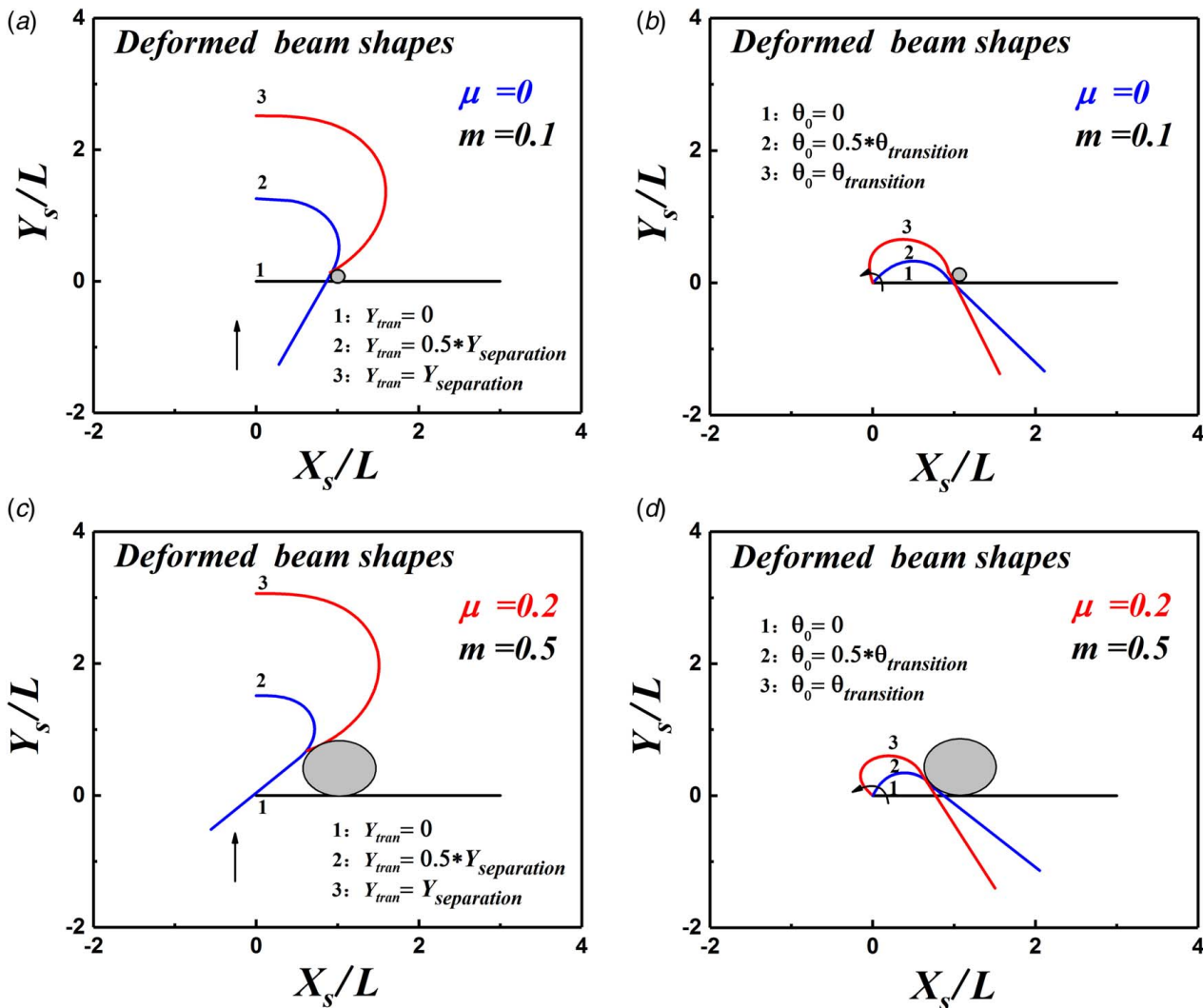
---

[3]See Note 2.

Fig. 5 Trajectory of whisker during contact under translation and rotation modes: (a) frictionless translation, (b) frictionless rotation, (c) frictional translation, and (d) frictional rotation
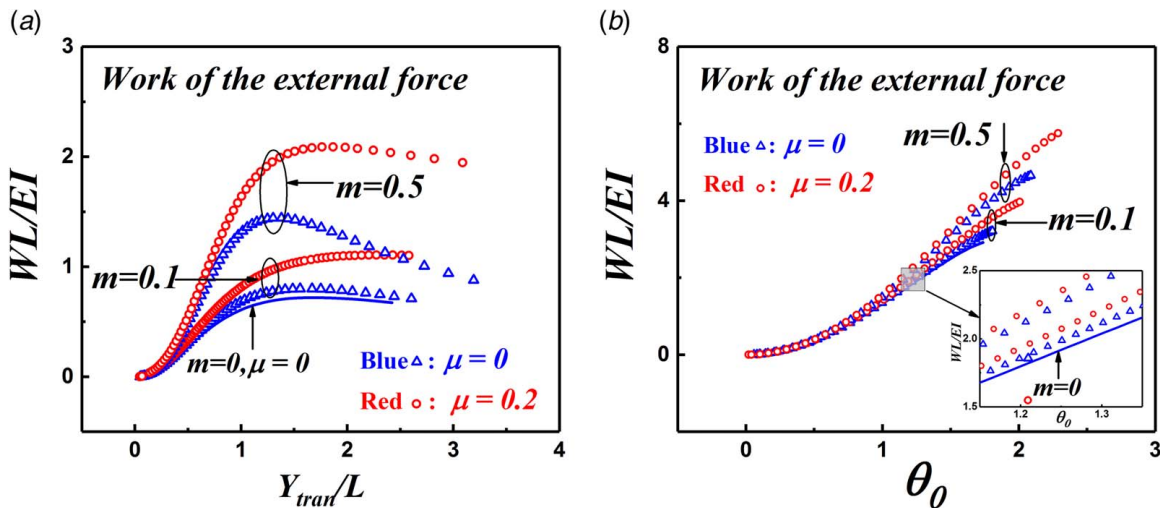

Fig. 6 Evolution of external work during contact: (a) translation, with respect to translation displacement and (b) rotation, with respect to rotation angle at fixed end. Solid line reprensents the cases of point contact without friction, $m = 0$ and $\mu = 0$.
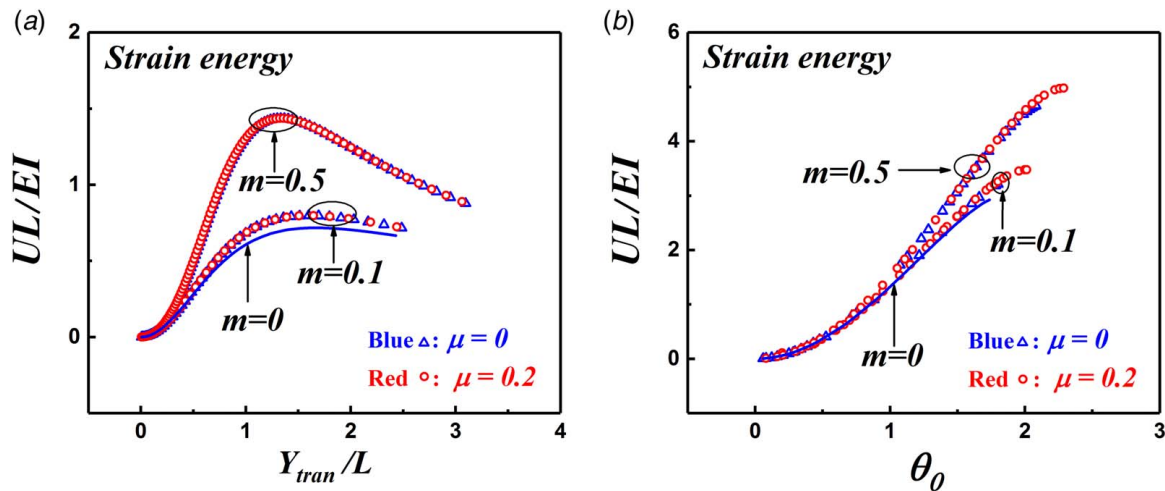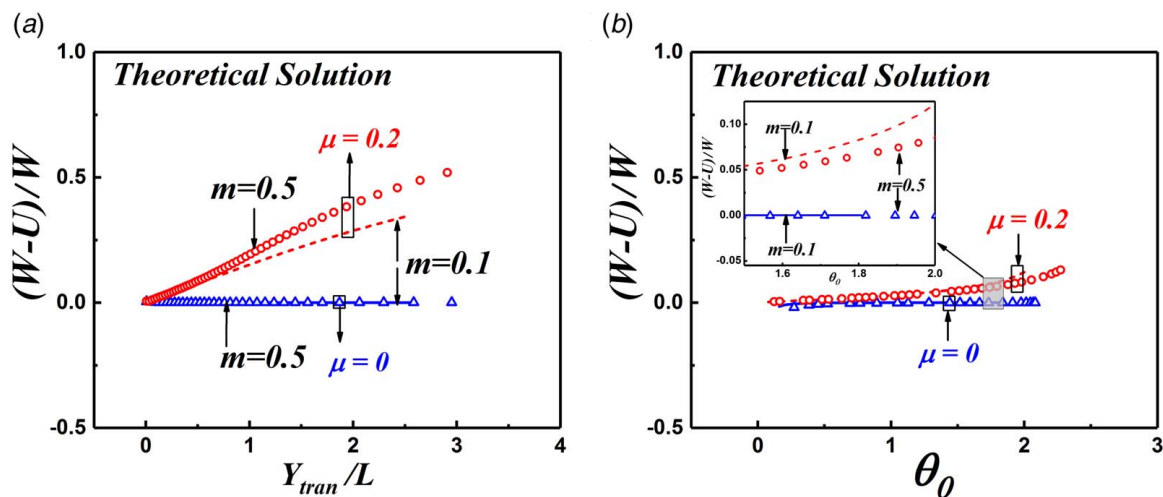
Fig. 7 Evolution of strain energy during contact: (*a*) translation, with respect to translation displacement and (*b*) rotation, with respect to rotation angle at fixed end. Solid line represents the cases of point contact without friction, $m = 0$ and $\mu = 0$.

Fig. 8 Ratio of friction dissipation to external work: (*a*) with respect to displacement for translation mode and (*b*) with respect to rotation angle for rotation mode

the time of passing over, and the $\theta_{critical}$ is defined as the value of rotation angle at the time of passing over. As shown in Fig. 10, before the beam length reaches a certain value, the detachment type is always "pull-off"; when beam length is larger than this value, the detachment type is "slip-off." When the "slip-off" occurs, $d_{critical}$, as well as $\theta_{critical}$, remains constant no matter how long the whisker length is.

Figure 10 shows that the detachment type is length dependent. To further compare the transition from "pull-off" with "slip-off" in Fig. 10, all the transition points from Fig. 10 are plotted in Fig. 11, which shows the transition length from "pull-off" to "slip-off." For the translation mode, the transition length is more than 3e5 times the initial contact length L, for different obstacle sizes and friction coefficients. This means that the "pull-off" might be the only way for detachment in the translation mode. While in the rotation mode, both "slip-off" and "pull-off" detachment can appear. The friction has little effect on the transition length of the rotation mode, and the transition length increases by approximately 20%, as the friction coefficient increases from 0.0 to 0.2 in the rotation mode.

It should be pointed out that, in a realistic situation, the ratio of L_w/L is mostly larger than 1.0 and cannot be larger than 10.0. Thus, in this case, "pull-off" might be the only detachment type for the translation mode. Both "slip-off" and "pull-off" detachment
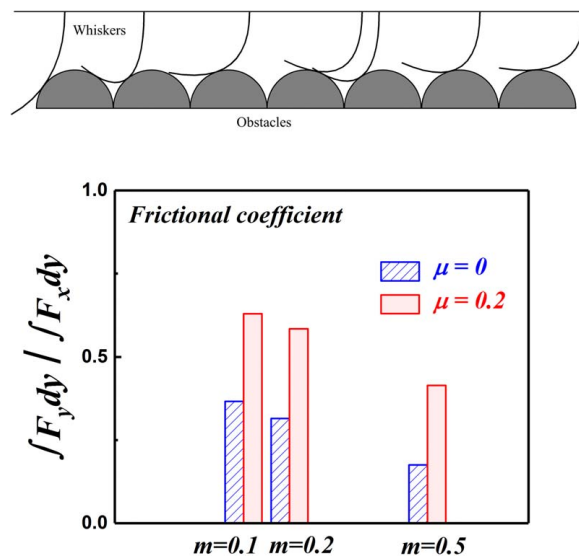

Fig. 9 Macro-scale friction coeffcient for bundle of whiskers sliding over rough surface with identical obstacles. Upper: typical contact situation.
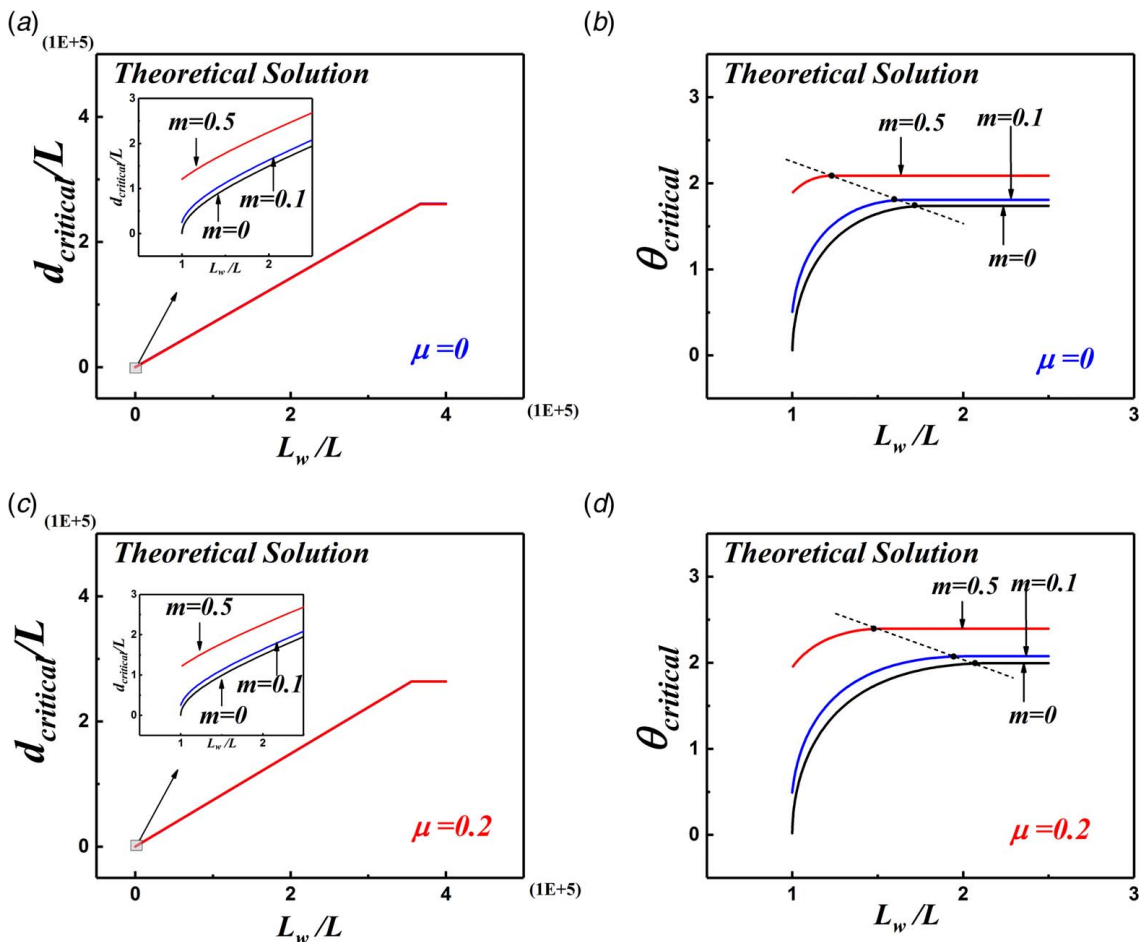
Fig. 10 Limits of translation displacement or rotation angle as a function of whisker length: (*a*) frictionless translation mode (insert shows enlarged image of initial stage), (*b*) frictionless rotation mode, (*c*) frictional translation mode (insert shows enlarged image of initial stage), and (*d*) frictional rotation mode. $d_{critical}$ is defined as value of displacement at moment of passing over and $\theta_{critical}$ as the value of rotation angle at moment of passing over

can appear in the rotation mode, because as shown in Fig. 11 the predicted transition whisker length in rotation mode is in the range of rom 1.0–2.5 times the initial contact length *L*.

3.3.2 Mechanism of "Slip-Off". In this section, an attempt is made to find the reason for "slip-off" detachment. As shown in Fig. 12, the force applied on the whisker can be decomposed into two components: one along the beam axis and the other

perpendicular to the axis. The present "slip-off" problem is similar to the buckling of a slender beam. The only difference here is that the beam is under an additional shear force Q_{shear}.

For further illustration, the axial and tangential forces when a whisker is in the moment of "slip-off" are shown in Figs. 13(*a*) and 13(*b*). The solid lines in both figures are obtained by the classical buckling theory of a slender beam with axial force. It is clear that the instability of buckling is not proper for the prediction
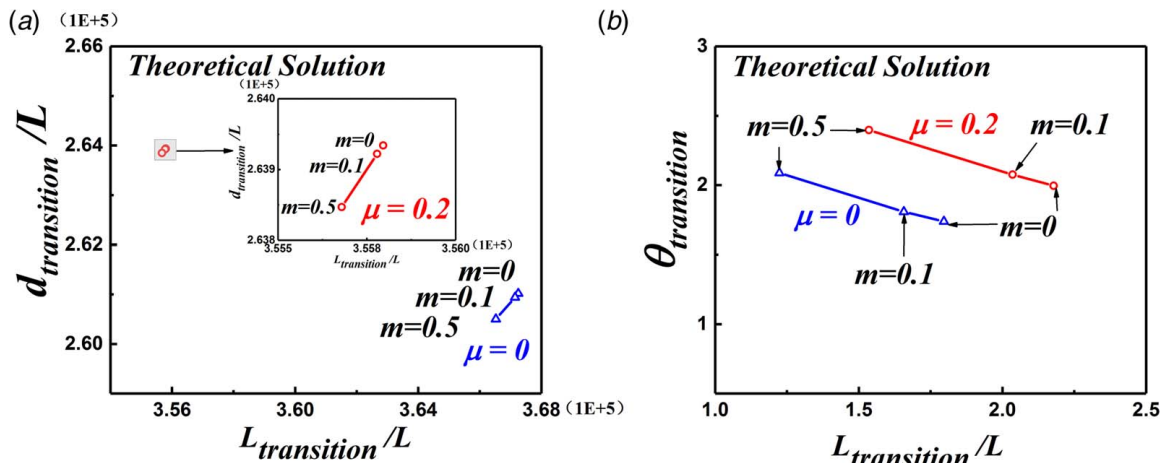

Fig. 11 Relative displacement limit of "slip-off" detachment: (*a*) translation and (*b*) rotation
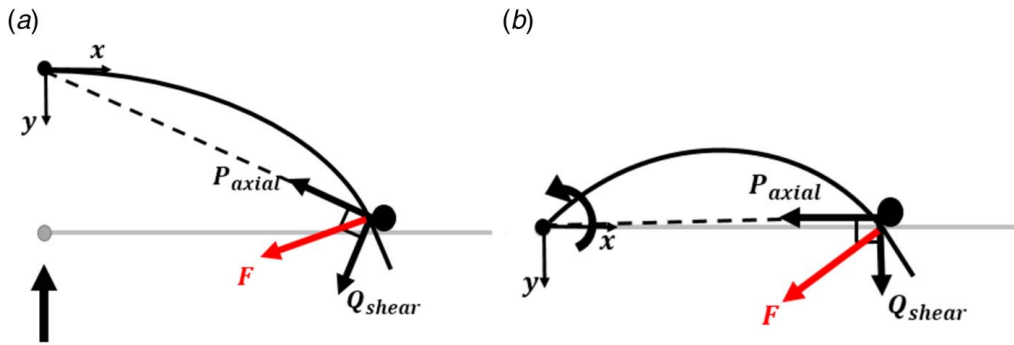
Fig. 12 Sketch of axial and shear loaded whisker during contact: (a) translation and (b) rotation
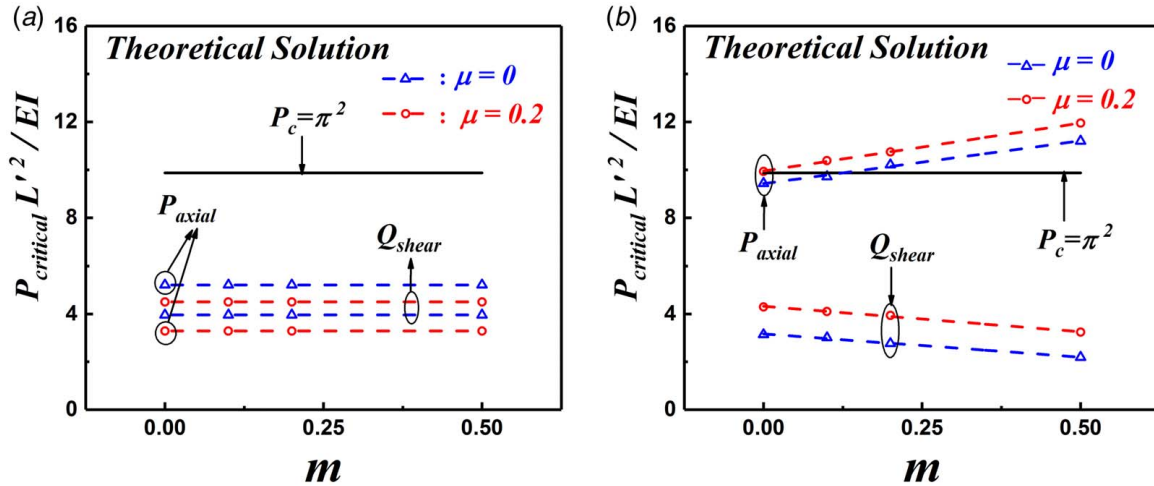

Fig. 13 Axial and shear forces at moment of "slip-off" as function of size coefficient m: (a) translation and (b) rotation

of "slip-off" in the translation mode, because compared with the axial force the tangential force is almost the same amount during "slip-off," so that the tangential effect on the instability of beam cannot be ignored. However, the instability of buckling provides a nice prediction of "slip-off" in the rotation mode because the axial force plays a dominant role during "slip-off" compared with the tangential force. Figure 13(b) also shows that the obstacle size slightly affects the prediction, and 20% deviation is also acceptable with a large obstacle ($m = 0.5$).

Based on the fact from Sec. 3.3.1, the "slip-off" seldom happens in the translation mode. Consequently, there is no need to consider the instability for the "slip-off" in the translation mode. Thus, we only need to consider "slip-off" for the rotation model, and the buckling theory shows a prediction with a deviation of less than 20%, so the buckling theory can be used for predicting the "slip-off" detachment for the rotational pass of a whisker over a round obstacle.

4 Conclusions

In this article, a contact model is developed to study the sliding behavior between a slender whisker and a round obstacle. The following conclusions are drawn.

(1) In comparison with the translation mode, only a small fraction of energy is dissipated by friction in the rotation mode, which is more energy efficient and preferred in nature.
(2) The present model reveals the dependency of the macro-scale friction coefficient of a bundle of whiskers sliding over a rough surface on the roughness of the surface: bigger is smoother.

(3) There are always two detachment types for the whisker–obstacle contact, the transition between which is length dependent. Results show that the "slip-off" style can seldom appear in the translation mode, while in the rotation mode, both "pull-off" and "slip-off" can appear and the transition whisker length is in the range of 1.0–2.5 times the initial contact length L.

Conflict of Interest

There are no conflicts of interest.

Data Availability Statement

The datasets generated and supporting the findings of this article are obtainable from the corresponding author upon reasonable request. The authors attest that all data for this study are included in the paper. Data provided by a third party listed in Acknowledgements. No data, models, or code were generated or used for this paper.

References

[1] Krupa, D. J., Matell, M. S., Brisben, A. J., Oliveira, L. M., and Nicolelis, M. A. L., 2001, "Behavioral Properties of the Trigeminal Somatosensory System in Rats Performing Whisker-Dependent Tactile Discriminations," J. Neurosci., **21**(15), pp. 5752–5763.

[2] Szwed, M., Bagdasarian, K., Blumenfeld, B., Barak, O., Derdikman, D., and Ahissar, E., 2006, "Responses of Trigeminal Ganglion Neurons to the Radial Distance of Contact During Active Vibrissal Touch," J. Neurophysiol., **95**(2), pp. 791–802.

[3] McConney, M. E., Schaber, C. F., Julian, M. D., Eberhardt, W. C., Humphrey, J. A. C., Barth, F. G., and Tsukruk, V. V., 2009, "Surface Force Spectroscopic Point Load Measurements and Viscoelastic Modelling of the Micromechanical Properties of Air Flow Sensitive Hairs of a Spider (Cupiennius Salei)," J. R. Soc. Interface, **6**(37), pp. 681–694.

[4] Astreinidi Blandin, A., Bernardeschi, I., and Beccai, L., 2018, "Biomechanics in Soft Mechanical Sensing: From Natural Case Studies to the Artificial World," Biomimetics (Basel), **3**(4), pp. 1–29.

[5] Seale, M., Cummins, C., Viola, I. M., Mastropaolo, E., and Nakayama, N., 2018, "Design Principles of Hair-Like Structures as Biological Machines," J. R. Soc. Interface, **15**(142), p 20180206.

[6] Solomon, J. H., and Hartmann, M. J., 2006, "Biomechanics: Robotic Whiskers Used to Sense Features," Nature, **443**(7111), pp. 525–525.

[7] Kaneko, M., Kanayama, N., and Tsuji, T., 1998, "Active Antenna for Contact Sensing," IEEE Trans. Rob. Autom., **14**(2), pp. 278–291.

[8] Ritt, J. T., Andermann, M. L., and Moore, C. I., 2008, "Embodied Information Processing: Vibrissa Mechanics and Texture Features Shape Micromotions in Actively Sensing Rats," Neuron, **57**(4), pp. 599–613.

[9] Birdwell, J. A., Solomon, J. H., Thajchayapong, M., Taylor, M. A., Cheely, M., Towal, R. B., Conradt, J., and Hartmann, M. J. Z., 2007, "Biomechanical Models for Radial Distance Determination by the Rat Vibrissal System," J. Neurophysiol., **98**(4), pp. 2439–2455.

[10] Solomon, J. H., and Hartmann, M. J., 2011, "Radial Distance Determination in the Rat Vibrissal System and the Effects of Weber's Law," Philos. Trans. R. Soc. Lond. B Biol. Sci., **366**(1581), pp. 3049–3057.

[11] Quist, B. W., and Hartmann, M. J., 2012, "Mechanical Signals at the Base of a Rat Vibrissa: The Effect of Intrinsic Vibrissa Curvature and Implications for Tactile Exploration," J. Neurophysiol., **107**(9), pp. 2298–2312.

[12] Vaziri, A., Jenks, R. A., Boloori, A.-R., and Stanley, G. B., 2007, "Flexible Probes for Characterizing Surface Topology: From Biology to Technology," Exp. Mech., **47**(3), pp. 417–425.

[13] Clements, T. N., and Rahn, C. D., 2006, "Three-Dimensional Contact Imaging With an Actuated Whisker," IEEE Trans. Rob., **22**(4), pp. 844–848.

[14] Hires, S. A., Pammer, L., Svoboda, K., and Golomb, D., 2013, "Tapered Whiskers Are Required for Active Tactile Sensation," Elife, **2**, p. e01350.

[15] Solomon, J. H., and Hartmann, M., 2008, "Artificial Whiskers Suitable for Array Implementation: Accounting for Lateral Slip and Surface Friction," IEEE Trans. Rob., **24**(5), pp. 1157–1167.

[16] Maoiléidigh, D. Ó., Nicola, E. M., and Hudspeth, A., 2012, "The Diverse Effects of Mechanical Loading on Active Hair Bundles," Proc. Natl. Acad. Sci. USA, **109**(6), pp. 1943–1948.

[17] Batista, M., 2015, "Large Deflections of a Beam Subject to Three-Point Bending," Int. J. Non-Linear Mech., **69**, pp. 84–92.

[18] Howell, L. L., and Midha, A., 1995, "Parametric Deflection Approximations for End-Loaded, Large-Deflection Beams in Compliant Mechanisms," ASME J. Mech. Des., **117**(1), pp. 156–165.

[19] Freeman, J., 1946, "LXXXIX. Mathematical Theory of Deflection of Beam," London, Edinburgh, Dublin Philosophical Magazine J. Sci., **37**(275), pp. 855–862.